Available online at www.sciencedirect.com

ScienceDirect

journal homepage: www.elsevier.com/locate/he

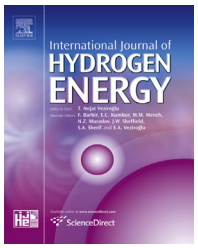

Effects of substituting Cu for Sn on the microstructure and hydrogen absorption properties of Co-free AB_5 alloys

Julio Cesar Serafim Casini [a,*], *Franks Martins Silva* [a], *Zai-ping Guo* [b], *Hua Kun Liu* [b], *Rubens Nunes Faria* [c], *Hidetoshi Takiishi* [c]

[a] *Federal Institute of Education, Science and Technology of Rondônia, RO 76820-441, Brazil*
[b] *Institute for Semiconducting and Electronic Materials, University of Wollongong, NSW 2522, Australia*
[c] *Materials Science and Technology Center, Nuclear and Energy Research Institute, University of São Paulo, SP 05508-900, Brazil*

ARTICLE INFO

Article history:
Received 16 June 2015
Received in revised form
27 May 2016
Accepted 15 July 2016
Available online 30 July 2016

Keywords:
Hydrogen storage alloys
Microstructure
Ni–MH batteries
Rare earths
PCI characteristics

ABSTRACT

The effects of substituting Cu for Sn on the microstructure, hydrogen storage capacity of $La_{0.7}Mg_{0.3}Al_{0.3}Mn_{0.4}Sn_{0.5-x}Cu_xNi_{3.8}$ alloys (where X = 0.0, 0.1, 0.2, 0.3, and 0.5) alloys were investigated with X-ray diffraction (XRD), scanning electron microscopy (SEM), energy dispersive X-ray spectroscopy (EDS), and pressure-composition isotherms (PCIs). The alloys were mainly composed of three phases: $LaNi_5$, $MgNi_2$, and LaNiSn. However, the $La_{0.7}Mg_{0.3}Al_{0.3}Mn_{0.4}Cu_{0.5}Ni_{3.8}$ alloy (X = 0.5) exhibited a (La, Mg)Ni_3 phase when studied with SEM. The PCI tests showed that increasing the Cu content increases the maximum hydrogen storage capacity.

Introduction

Over the years, $LaNi_5$-based alloys have been the subject of many studies. One successful application of these alloys is as the active material in the negative electrodes of Ni–MH batteries. The ability of AB_5 alloys to absorb hydrogen at room temperature is their main advantage. When used in Ni–MH batteries, the $LaNi_5$-based alloys have been partially modified by replacing certain elements to improve the kinetics of the hydrogen absorption and desorption processes, increase the cycle life, improve corrosion resistance, etc. Co, Al, Mn, and Mg are invariably present in such alloys [1–4].

The wider use of Ni–MH batteries has become a concern in recent years because of the high cost of some of the elements employed to create the negative electrode. However, some researchers have been investigating low-Co and Co-free alloys. Both Ni and Co have been replaced with other elements, including Fe, Cu, and Si, to obtain the same hydrogen absorption properties but with low-cost alloys [5–7]. The use of Nb as a replacement has been reported for the $La_{0.7}Mg_{0.3}Al_{0.3}Mn_{0.4}X_{0.5}Ni_{3.8}$ alloys (X = Co, Nb). However, the microstructure

* *Corresponding author*. Av. Calama, 4985, Flodoaldo Pontes Pinto, 76820-441 Porto Velho, RO, Brazil. Fax: +55 69 21828901.
E-mail address: julio.casini@ifro.edu.br (J.C.S. Casini).
http://dx.doi.org/10.1016/j.ijhydene.2016.07.107

of the Nb-doped alloys contained the $NbNi_3$ phase, which is associated with a decrease in the discharge capacity of a battery [8]. Recently, the effects of substituting Sn for Co in AB_5-type $La_{0.7}Mg_{0.3}Al_{0.3}Mn_{0.4}Co_{0.5-x}Sn_xNi_{3.8}$ hydrogen storage alloys have been reported. It was found that a new phase, LaNiSn, was formed as the Sn content increased [9].

Cu has been successfully introduced to $LaNi_{4.7}Al_{0.3}$ metal-hydride electrodes by using Cu-coated alloy powders during the fabrication process [10]. Furthermore, it has been shown that substituting Cu for Ni affects the hydrogen storage capacity of the cast and quenched $La_{0.7}Mg_{0.3}Co_{0.45}Cu_xNi_{2.55-x}$ alloys, but it significantly improves their stability [11]. In this study, the microstructure, phase composition, and hydrogen absorption properties of AB_5-type $La_{0.7}Mg_{0.3}Al_{0.3}Mn_{0.4}Sn_{0.5-x}Cu_xNi_{3.8}$ hydrogen storage alloys have been systematically investigated.

Experimental details

The nominal composition of the alloys studied can be represented by the following general formula: $La_{0.7}Mg_{0.3}Al_{0.3}Mn_{0.4}Sn_{0.5-x}Cu_xNi_{3.8}$, where X = 0.0, 0.1, 0.2, 0.3, and 0.5. The purity of all the elements used was at least 99.9%. The alloys were prepared by induction heating in a water-cooled Cu crucible under an Ar atmosphere. The ingots were re-melted twice to achieve homogeneity.

For the pressure-composition isotherm (PCI) and X-ray diffraction (XRD) measurements, the alloys were mechanically pulverized in an agate mortar and sieved through a 200-size mesh (particle size <75 μm). The PCI tests were conducted with a gas reaction controller from Advanced Materials Corporation. Prior to each measurement, a sample was placed in a vessel that was then evacuated at 30 °C for 1 h with a rotary vacuum pump, which was activated for 5 cycles. The PCI tests were performed at 30 °C until a hydrogen pressure of 3 MPa was reached. The hydrogen gas (purity = >99.99%) was supplied from a cylinder. The hysteresis between the hydrogen absorption and desorption processes was measured to evaluate the reversibility of the hydriding process. The PCI hysteresis factor (H_f) was calculated with Equation (1):

$$H_f = ln\left(\frac{P_a}{P_d}\right) \quad (1)$$

where P_a and P_d are the absorption and desorption equilibrium pressures at a hydrogen storage capacity of 50%, respectively. The slope factor (S_f) can be used to quantify the plateauing hydrogen absorption performance. The S_f value is calculated by taking the ratio of the capacities between the middle region (defined as between 0.01 and 0.5 MPa) and the entire reversible region.

The phase identification was performed with a GBC MMA X-ray diffractometer using Cu Kα radiation at 40 kV and 25 mA. The scan rate was 0.25° per min, with a step of 0.02° from 10° to 100°. The phases present were identified with the Crystallographica Search-Match software (CSM, PDF release 2002). The Rietveld refinements were performed with Materials Studio 4.3. The microstructure and composition of the alloys were examined with a scanning electron microscopy (SEM) setup equipped for energy dispersive X-ray spectroscopy (EDS).

For the electrochemical measurements, the alloys were firstly mechanically pulverized and sieved through 200 mesh (<75 μm). All test electrodes were prepared by mixing alloy powder and nickel powder (<3 μm) with a weight ratio of 1:4. The mixture was cold pressed in nickel gauze (40 mesh) under a pressure of 15 MPa (about 1 cm^2 in area and 0.1 mm in thickness). The discharge capacity of each electrode was measured in a flooded cell configuration using $Ni(OH)_2$/NiOOH as the counter electrode and 6 M KOH solution as the electrolyte. The system was charged at 100 mA/g for 5 h followed by a 10 min rest and then discharged at 50 mA/g to the cut-off potential of 0.8 V.

High rate dischargeability (HRD) represents the kinetic property of hydrogen storage alloy electrodes and was calculated using the following formula:

$$HRD = \frac{C_d}{C_d + C_{50}} \times 100\% \quad (2)$$

where Cd is discharge capacity with a cut-off potential of 0.8 V at the discharge current density Id; and C_{50} is the residual discharge capacity with a cut-off potential of 0.8 V at the discharge current density I = 50 mA/g after the electrode has been fully discharged at Id. HRD values were calculated when each electrochemical cell became active.

Results and discussion

Microstructure and phase composition

The XRD patterns of the $La_{0.7}Mg_{0.3}Al_{0.3}Mn_{0.4}Sn_{0.5-x}Cu_xNi_{3.8}$ hydrogen storage alloys, where X = 0.0–0.5, are shown in Fig. 1. These patterns show that the alloys are mainly composed of $LaNi_5$ (with a $CaCu_5$-type hexagonal structure), $MgNi_2$, and LaNiSn phases. The X = 0.5 alloy exhibits a (La, Mg)Ni_3 phase, which has a $PuNi_3$-type rhombohedral structure. The lattice parameters, unit cell volumes, and abundance of each phase

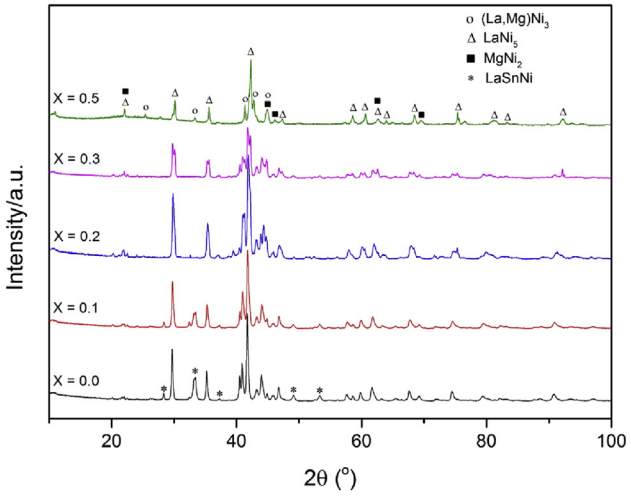

Fig. 1 – XRD patterns of the $La_{0.7}Mg_{0.3}Al_{0.3}Mn_{0.4}Sn_{0.5-x}Cu_xNi_{3.8}$ hydrogen storage alloys, where X = 0.0–0.5.

in the various alloys tested are listed in Table 1, which were obtained from the Rietveld refinements of the XRD patterns. It can be seen that the *a* and *c* parameters, as well as the unit cell volume, of the $LaNi_5$ phase decrease with increasing Cu content. This is because the atomic radius of Cu (1.28 Å) is smaller than that of Sn (1.45 Å). The $LaNi_5$ content increases from 53.42% (X = 0.0) to 78.30% (X = 0.3), and then decreases to 55.65% (X = 0.5). This final decrease can be explained by the formation of the (La, Mg)Ni_3 phase. The LaNiSn content decreases from 18.96% (X = 0.0) to 5.16% (X = 0.3), and obviously there is no evidence of this phase in the X = 0.5 alloy, where Sn has been completely replaced by Cu.

The SEM micrographs of the $La_{0.7}Mg_{0.3}Al_{0.3}Mn_{0.4}Sn_{0.5-x}Cu_xNi_{3.8}$ hydrogen storage alloys (X = 0.0–0.5) are shown in Fig. 2. By combining these SEM micrographs with the results of the EDS analysis, which are given in Table 2, it was possible to identify the composition of each phase present in the XRD patterns. The La- and Ni-rich phase (light grey regions) is the $LaNi_5$ phase, while the second phase is mostly composed of Mg and Ni ($MgNi_2$ phase, dark regions). High concentrations of Sn were found in the white regions of the microstructure. In a previous study, a similar phase appeared when Sn substitutions were made, and as the Sn content gradually increased, more of these fine grains were found [9]. This corresponds well with a previous study on $LaNi_{4.0}Al_{0.2}Fe_{0.4}Cu_{0.4-x}Sn_x$ alloys [12]. In the Sn-free alloy (X = 0.5, $La_{0.7}Mg_{0.3}Al_{0.3}Mn_{0.4}Cu_{0.5}Ni_{3.8}$; Fig. 2(e)), the pseudo-binary phase (La, Mg)Ni_3 is present; there is no evidence of this phase in the other alloys. De Negri et al. investigated the ternary phase diagram of the La–Mg–Ni system and reported a microstructure for the $La_{8.5}Ni_{76.5}Mg_{15.0}$ alloy that is quite similar to that found in this work [13].

PCI tests

The PCI curves of the $La_{0.7}Mg_{0.3}Al_{0.3}Mn_{0.4}Sn_{0.5-x}Cu_xNi_{3.8}$ hydrogen storage alloys (X = 0.0–0.5) at 30 °C are shown in Fig. 3. The maximum hydrogen storage capacity, H_f, and S_f values calculated for each alloy from the PCI curves are shown in Fig. 4. As can be seen, the maximum hydrogen storage capacity (wt %) of the alloys increases from 0.85 wt.% (X = 0.0) to 1.32 wt.% (X = 0.5), which can be explained by the decreasing concentration of the LaNiSn phase in the alloys; Jiangyuan et al. reported similar results [12]. In a previous study, the $(H/M)_{max}$ of the $La_{0.7}Mg_{0.3}Al_{0.3}Mn_{0.4}Co_{0.5}Ni_{3.8}$ alloy (a fully Co-doped alloy) was 1.48 wt.% [9]. Compared to the hydrogen capacity of the $La_{0.7}Mg_{0.3}Al_{0.3}Mn_{0.4}Cu_{0.5}Ni_{3.8}$ alloy (X = 0.5, 1.32 wt.%) in the present study, these values support the hypothesis that optimizing the $LaNi_5$ and (La, Mg)Ni_3 contents improves the hydrogen storage capacity [14].

As shown in Fig. 4, the reversibility of the hydrogen absorption and desorption processes, as represented by H_f, increases from 0.71 (X = 0.0) to 1.06 (X = 0.5). This means that the reversibility decreases as the Cu content increases because the reversibility is inversely proportional to H_f. In addition, the increase or decrease of H_f is directly related to the variation of the cell volume. Thus, the decreasing lattice parameters and cell volume of the $LaNi_5$ phase could explain the substantial increase in H_f, as shown in Fig. 5.

Furthermore, S_f decreases from 65.25% (X = 0.0) to 44.59% (X = 0.5), showing that the plateauing hydrogen absorption performance is improved by the addition of Cu. Huang et al. [15] and Zhou et al. [16] showed that H_f and S_f are strongly influenced by the homogeneity of an alloy. A homogenous composition and optimized structure are directly related to the plateauing hydrogen absorption performance. It is thought that the LaNiSn phase reduces the homogeneity of the phases. Therefore, decreasing the concentration of the LaNiSn phase enhances the homogeneity of the two phases that are involved in the hydrogen absorption process ($LaNi_5$ and (La, Mg)Ni_3), which in turn increases the maximum hydrogen storage capacity and decreases S_f.

Table 3 shows a comparison of the properties for the alloys tested in this study and those reported in a previous study [9]. It can be seen that Co substitution produces the best hydrogen storage capacity (1.48 wt.%), whereas Sn substitution produces the worst S_f value (65.24%). On the other hand, Cu substitution yields an alloy with a good overall performance.

Table 1 – The compositional and structural characteristics of the phases in the $La_{0.7}Mg_{0.3}Al_{0.3}Mn_{0.4}Sn_{0.5-x}Cu_xNi_{3.8}$ hydrogen storage alloys, where X = 0.0–0.5.

Sample	Phases	Space group (no.)	Parameter of fit (%)	Phase abundance (wt%)	Lattice parameters (Å)			Cell volume (Å^3)
					a	*b*	*c*	
X = 0.0	$LaNi_5$	P6/mmm (191)	R_{wp} = 7.8	53.42	5.088		4.107	92.08
	$MgNi_2$	P63/mmc (194)		27.8	4.813		15.731	315.59
	LaNiSn	Pnma (62)		18.96	7.672	4.915	7.357	277.42
X = 0.1	$LaNi_5$	P6/mmm (191)	R_{wp} = 8.2	67.98	5.082		4.103	91.77
	$MgNi_2$	P63/mmc (194)		16.18	4.816		15.367	308.66
	LaNiSn	Pnma (62)		15.83	7.597	4.675	7.480	265.66
X = 0.2	$LaNi_5$	P6/mmm (191)	R_{wp} = 8.3	73.27	5.072		4.088	91.07
	$MgNi_2$	P63/mmc (194)		16.35	4.829		15.642	315.88
	LaNiSn	Pnma (62)		10.36	7.552	4.382	7.514	248.65
X = 0.3	$LaNi_5$	P6/mmm (191)	R_{wp} = 9.2	78.30	5.066		4.078	90.63
	$MgNi_2$	P63/mmc (194)		16.52	4.855		15.878	324.11
	LaNiSn	Pnma (62)		5.17	7.529	4.339	7.590	247.95
X = 0.5	$LaNi_5$	P6/mmm (191)	R_{wp} = 6.7	55.65	5.050		4.046	89.35
	$MgNi_2$	P63/mmc (194)		7.19	5.092		15.842	355.72
	(La, Mg)Ni_3	$R\bar{3}$ m (166)		37.15	4.941		23.678	500.60

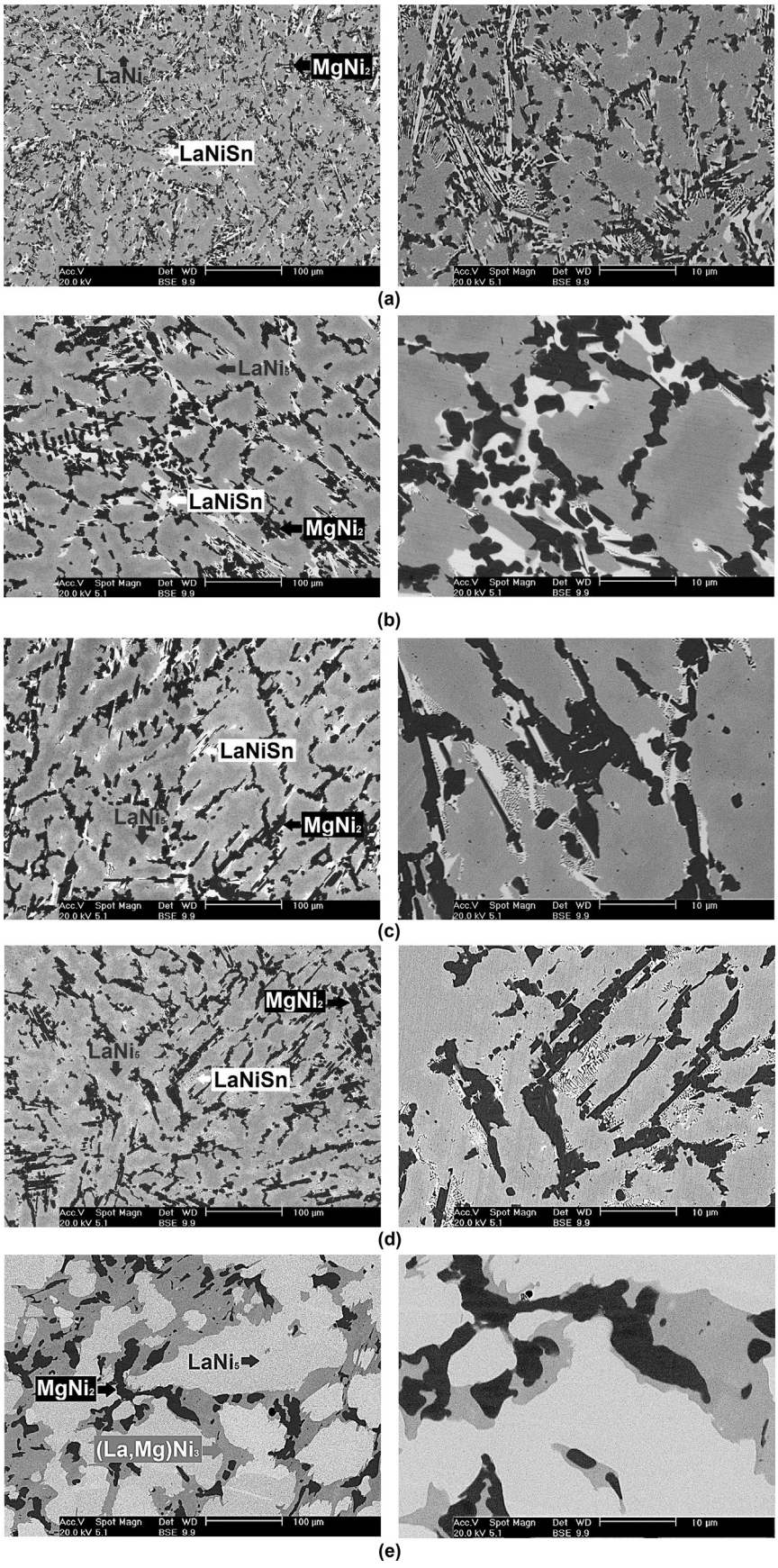

Fig. 2 – SEM micrographs showing general (left-hand side) and detailed (right-hand side) views of the $La_{0.7}Mg_{0.3}Al_{0.3}Mn_{0.4}Sn_{0.5-x}Cu_xNi_{3.8}$ alloys: (a) X = 0.0, (b) X = 0.1, (c) X = 0.2, (d) X = 0.3, and (e) X = 0.5.

Table 2 – EDS results for the different phases identified in the SEM micrographs of the $La_{0.7}Mg_{0.3}Al_{0.3}Mn_{0.4}Sn_{0.5-x}Cu_xNi_{3.8}$ hydrogen storage alloys, where X = 0.0–0.5.

Sample	Phase	Elements (at%)						
		La	Mg	Al	Mn	Sn	Cu	Ni
X = 0.0	$LaNi_5$	15.7	<1	4.4	3.5	6.9	–	68.9
	$MgNi_2$	<1	21.7	3.5	11.8	<1	–	61.5
	LaNiSn	19.8	4.1	2.3	3.2	20.4	–	50.2
X = 0.1	$LaNi_5$	14.2	2.7	4.8	3.3	3.7	1.2	70.1
	$MgNi_2$	<1	21.7	3.4	10.4	<1	1.5	61.5
	LaNiSn	19.5	4.6	2.5	3.4	22.3	<1	47.1
X = 0.2	$LaNi_5$	14.4	2.4	4.7	4.2	2.9	3.9	67.5
	$MgNi_2$	<1	21.2	3.7	9.8	<1	3.7	60.1
	LaNiSn	19.6	4.5	2.4	3.6	20.4	2.7	46.8
X = 0.3	$LaNi_5$	14.2	2.3	4.9	3.8	2.2	4.5	68.1
	$MgNi_2$	<1	21.2	3.5	10.2	<1	4.7	59.1
	LaNiSn	20.3	4.6	1.9	3.4	19.6	3.1	47.1
X = 0.5	$LaNi_5$	14.3	2.2	4.8	3.4	–	7.2	68.1
	$MgNi_2$	<1	23.3	3.3	9.9	–	6.2	57.0
	$(La, Mg)Ni_3$	9.1	12.9	3.7	6.5	–	8.7	59.1

The high cost of Co will play a decisive role in the selection of the dopant(s), with this study showing that Cu is the better choice compared to Sn.

Electrochemical characterization

The complete study of the electrochemical performance of $La_{0.7}Mg_{0.3}Al_{0.3}Mn_{0.4}Sn_{0.5-x}Cu_xNi_{3.8}$ alloys (X = 0.0–0.5) could be founded in previous work [17]. Table 4 shows a comparison of the electrochemical properties of each alloy composition in this study, additionally an alloy reported in previous work ($La_{0.7}Mg_{0.3}Al_{0.3}Mn_{0.4}Co_{0.5}Ni_{3.8}$) [9]. The maximum discharge capacity (C_{max}) increase from 239.8 mA h/g (x = 0.0) to 305.2 mA h/g (x = 0.5) with increase of copper in the alloys.

The correlation between the hydrogen capacity and the maximum discharge capacity (C_{max}) of the $La_{0.7}Mg_{0.3}Al_{0.3}Mn_{0.4}Sn_{0.5-x}Cu_xNi_{3.8}$ (x = 0.0–0.5) alloys, are shown in Fig. 6.

The increase of electrochemical behavior may be noted at discharge capacity retention (C_{100}/C_{max}) and at high rate dischargeability (HRD). For example, the HRD at 1400 mA/g (HRD_{1400}) increase drastically from 25.7% (x = 0.0) to 80.6% (x = 0.5). It is evident that Co substitution resulted in improved discharge capacity (337.1 mA h/g) over Sn and Cu substitution (Table 4). The Sn-substituted alloy exhibited the lowest HRD (25.7%). Cu substitution yielded good overall electrochemical performance of the negative electrode alloys, showing only a small discharge capacity loss of 9.5% with an 11.6% enhancement of discharge capacity retention at the 100th

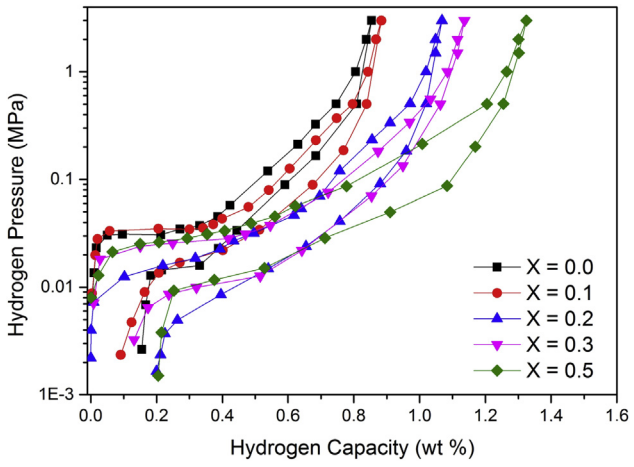

Fig. 3 – PCI curves of the $La_{0.7}Mg_{0.3}Al_{0.3}Mn_{0.4}Sn_{0.5-x}Cu_xNi_{3.8}$ alloys (X = 0.0–0.5) at 30 °C.

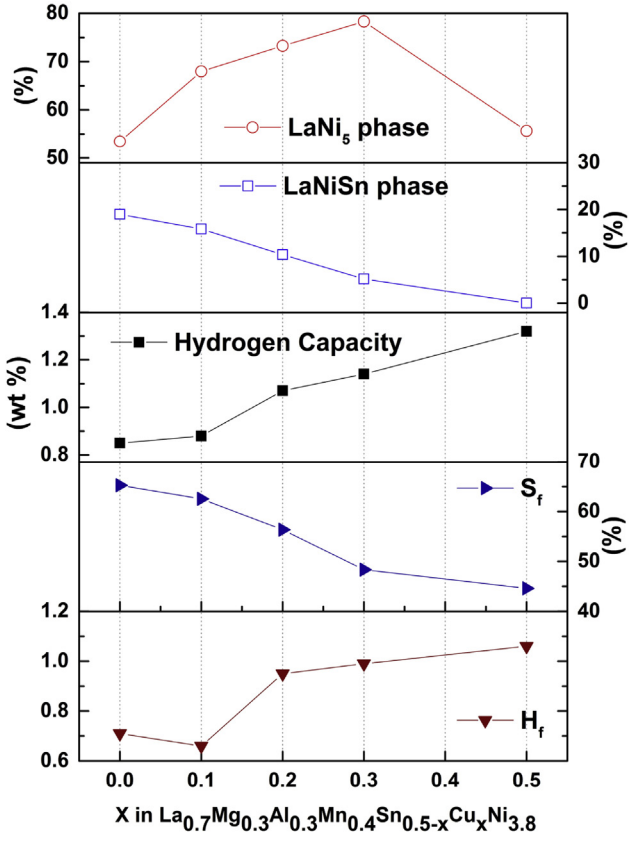

Fig. 4 – $(H/M)_{max}$, H_f, and S_f values of the $La_{0.7}Mg_{0.3}Al_{0.3}Mn_{0.4}Sn_{0.5-x}Cu_xNi_{3.8}$ hydrogen storage alloys, where X = 0.0–0.5.

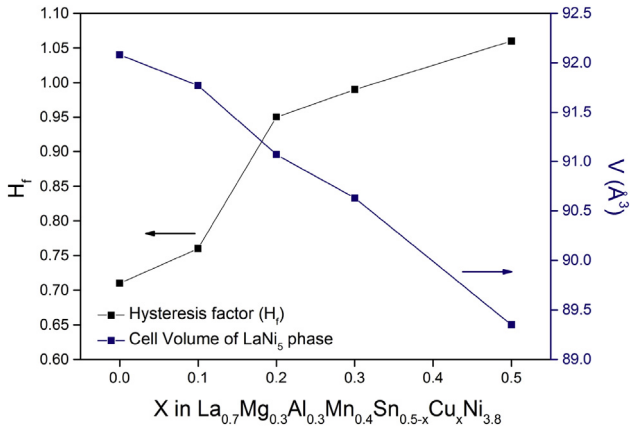

Fig. 5 – Relationship between Hf and cell volume of $LaNi_5$ phase of the $La_{0.7}Mg_{0.3}Al_{0.3}Mn_{0.4}Sn_{0.5-x}Cu_xNi_{3.8}$ hydrogen storage alloys, where X = 0.0–0.5.

Table 3 – $(H/M)_{max}$, H_f, and S_f values of the $La_{0.7}Mg_{0.3}Al_{0.3}Mn_{0.4}M_{0.5}Ni_{3.8}$ (M = Sn, Cu, or Co) alloys.

Alloy	Hydrogen capacity (wt%)	H_f	S_f (%)
$La_{0.7}Mg_{0.3}Al_{0.3}Mn_{0.4}Sn_{0.5}Ni_{3.8}$	0.85	0.71	65.24
$La_{0.7}Mg_{0.3}Al_{0.3}Mn_{0.4}Cu_{0.5}Ni_{3.8}$	1.32	1.06	44.59
$La_{0.7}Mg_{0.3}Al_{0.3}Mn_{0.4}Co_{0.5}Ni_{3.8}$ [9]	1.48	1.06	38.85

Table 4 – Electrochemical properties of $La_{0.7}Mg_{0.3}Al_{0.3}Mn_{0.4}Sn_{0.5-x}Cu_xNi_{3.8}$ alloys, where X = 0.0–0.5, and a comparison with $La_{0.7}Mg_{0.3}Al_{0.3}Mn_{0.4}Co_{0.5}Ni_{3.8}$.

Alloy	C_{max} (mA h/g)	C_{100}/C_{max}	HRD_{1400}
$La_{0.7}Mg_{0.3}Al_{0.3}Mn_{0.4}Sn_{0.5}Ni_{3.8}$	239.8	78.0	25.7
$La_{0.7}Mg_{0.3}Al_{0.3}Mn_{0.4}Sn_{0.4}Cu_{0.1}Ni_{3.8}$	251.2	78.7	37.1
$La_{0.7}Mg_{0.3}Al_{0.3}Mn_{0.4}Sn_{0.3}Cu_{0.2}Ni_{3.8}$	279.1	79.8	54.5
$La_{0.7}Mg_{0.3}Al_{0.3}Mn_{0.4}Sn_{0.2}Cu_{0.3}Ni_{3.8}$	301.1	80.5	66.4
$La_{0.7}Mg_{0.3}Al_{0.3}Mn_{0.4}Cu_{0.5}Ni_{3.8}$	305.2	81.8	80.6
$La_{0.7}Mg_{0.3}Al_{0.3}Mn_{0.4}Co_{0.5}Ni_{3.8}$ [9]	337.1	70.2	68.4

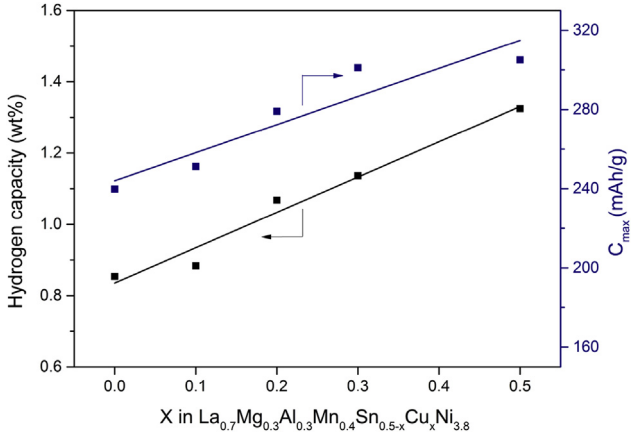

Fig. 6 – The Hydrogen capacity and the electrochemical discharge capacity of the $La_{0.7}Mg_{0.3}Al_{0.3}Mn_{0.4}Sn_{0.5-x}Cu_xNi_{3.8}$ (x = 0.0–0.5) alloys.

cycle, and a 12.2% increase in HRD at a discharge current density of 1400 mA/g.

Conclusions

This paper has shown that substituting Cu for Sn has substantial effects on the microstructure and hydrogen storage performance of $La_{0.7}Mg_{0.3}Al_{0.3}Mn_{0.4}Sn_{0.5-x}Cu_xNi_{3.8}$ alloys (X = 0.0–0.5). The $La_{0.7}Mg_{0.3}Al_{0.3}Mn_{0.4}Cu_{0.5}Ni_{3.8}$ alloy, i.e., X = 0.5, showed the best hydrogen storage capacity (1.32 wt.%). Three main phases were found in these alloys: $LaNi_5$, $MgNi_2$ and LaNiSn. By increasing the Cu content, the concentration of the LaNiSn phase decreased. However, in the X = 0.5 alloy, a new phase, $(La, Mg)Ni_3$, had formed. The values of $(H/M)_{max}$ and H_f increased with increasing Cu content. On the other hand, the S_f values decreased as the Cu content increased, indicating a significant improvement in the homogeneity of the alloys.

Acknowledgments

The authors wish to thank the Institute for Superconducting and Electronic Materials (ISEM) of the University of Wollongong, the Nuclear and Energy Research Institute (IPEN) of the University of São Paulo, and Federal Institute of Education, Science and Technology of Rondônia for their financial support. The authors also wish to thank the National Council for Scientific and Technological Development of Brazil for the scholarships granted to Casini, J.C.S. (CNPq - SWE/CSF 237694/2012-3) and financial support (CNPq 472504/2010-0) and (CNPq 471889/2013-0).

REFERENCES

[1] Yang S, Han S, Song J, Li Y. Influences of molybdenum substitution for cobalt on the phase structure and electrochemical kinetic properties of AB_5-type hydrogen storage alloys. J Rare Earths 2011;29:692–7.
[2] Liu Y, Pan H, Gao M, Wang Q. Advanced hydrogen storage alloys for Ni/MH rechargeable batteries. J Mater Chem 2011;21:4743–55.
[3] Sakai T, Yoshinaga H, Migamura H, Kurigama N, Ishikawa H. Rechargeable hydrogen batteries using rare-earth-based hydrogen storage alloys. J Alloys Compd 1992;180:37–54.
[4] Cuscueta DJ, Melnichuk M, Peretti HA, Salva HR, Ghilarducci AA. Magnesium influence in the electrochemical properties of La–Ni base alloy for Ni–MH batteries. Int J Hydrogen Energy 2008;33:3566–70.
[5] Tang W, Gai Y, Zheng H. Deterioration of copper-containing mischmetal-nickel-based hydrogen absorption electrode materials. J Alloys Compd 1995;224:292–8.
[6] Weizhong T, Yingxin G, Haoyu Z. Electrode stabilities of copper-containing misch metal-nickel-based hydride forming alloys. J Appl Electrochem 1995;25:874–80.
[7] Sakai T, Miyamura T, Kuriyama N, Kato A, Oguro K, Ishikawa H, et al. The influence of small amounts of added elements on various anode performance characteristics for $LaNi_{2.5}Co_{2.5}$-based alloys. J Less Common Metals 1990;159:127–39.

[8] Ferreira EA, Serra JM, Casini JCS, Takiishi H, Faria RN. Microstructure and electrochemical properties of a LaMgAlMnCoNi based alloy for Ni/MH batteries. Mater Sci Forum 2012;727–728:80–4.
[9] Casini JCS, Ferreira EA, Guo Z, Liu HK, Faria RN, Takiishi H. Effect of Sn substitution for Co on microstructure and electrochemical performance of AB_5 type $La_{0.7}Mg_{0.3}Al_{0.3}Mn_{0.4}Co_{0.5-x}Sn_xNi_{3.8}$ (x=0–0.5) alloys. Trans Nonferrous Metals Soc China 2015;25:520–6.
[10] Feng F, Northwood DO. Improved performance of a metal hydride electrode for nickel/metal hydride batteries through copper-coating. Surf Coatings Technol 2003;167:263–8.
[11] Zhang Y, Donga X, Wang G, Guo S, Ren J, Wang X. Microstructure and electrochemical performances of $La_{0.7}Mg_{0.3}Ni_{2.55-x}Co_{0.45}Cu_x$ (x = 0–0.4) hydrogen storage alloys prepared by casting and rapid quenching. J Alloys Compd 2006;417:224–9.
[12] Ren J, Zhanga T, Feng M, Wang G, Zhao X, Wang X. Microstructures and electrochemical properties of cobalt-free $LaNi_{4.0}Al_{0.2}Fe_{0.4}C_{u0.4-x}Sn_x$ (x = 0 ~ 0.4) electrode alloys prepared by casting. J Rare Earths 2006;24:574–8.
[13] De Negri S, Giovannini M, Saccone A. Phase relationships of the La–Ni–Mg system at 500 °C from 66.7 to 100 at.% Ni. J Alloys Compd 2007;439:109–13.
[14] Liu Y, Pan H, Zhu Y, Li R, Lei Y. Influence of Mn content on the structural and electrochemical properties of the $La_{0.7}Mg_{0.3}Ni_{4.25-x}Co_{0.75}Mn_x$ hydrogen storage alloys. Mater Sci Eng A 2004;372:163–72.
[15] Hunag T, Han J, Zhang Y, Yu J, Sun G, Ren H, et al. Study on the structure and hydrogen absorption–desorption characteristics of as-cast and annealed $La_{0.78}Mg_{0.22}Ni_{3.48}Co_{0.22}Cu_{0.12}$ alloys. J Power Sources 2011;196:9585–9.
[16] Zhou Z, Song Y, Cui S, Huang C, Qian W, Lin C, et al. Effect of annealing treatment on structure and electrochemical performance of quenched $MmNi_{4.2}Co_{0.3}Mn_{0.4}Al_{0.3}Mg_{0.03}$ hydrogen storage alloy. J Alloys Compd 2010;501:47–53.
[17] Casini JCS, Guo Z, Liu HK, Faria RN, Takiishi H. Effects of Cu substitution for Sn on the electrochemical performance of $La_{0.7}Mg_{0.3}Al_{0.3}Mn_{0.4}Sn_{0.5-x}Cu_xNi_{3.8}$ (x = 0–0.5) alloys for Ni-MH batteries. Batteries 2015;1:3–10.